

HERA: Illuminating Our Early Universe

For the Mid-Scale Science Projects category of the Mid-Scale Innovations Program

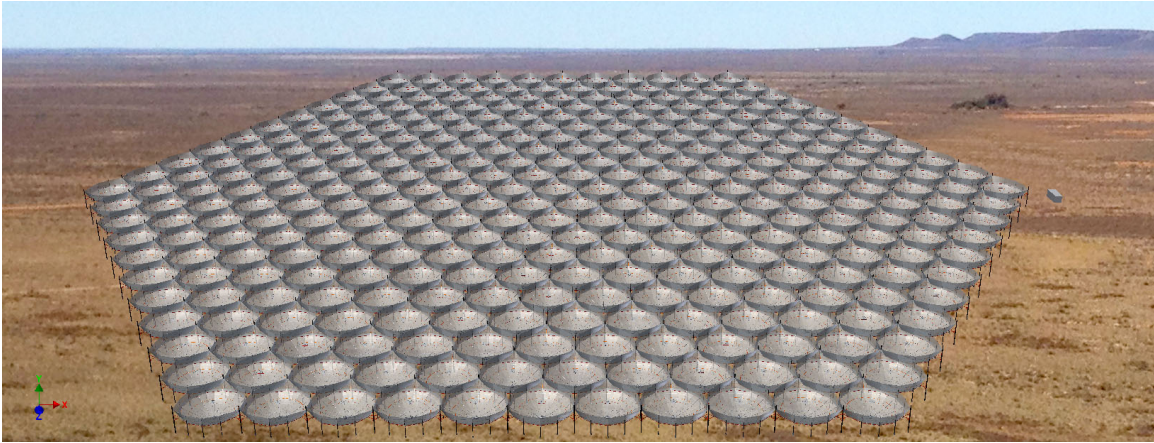


Fig. 1.— The proposed array of 331 14 m-diameter zenith-pointing dishes in the Karoo Radio Astronomy Reserve in the Northern Cape of South Africa.

1. Overview of this Proposal

The Hydrogen Epoch of Reionization Arrays (HERA) roadmap is a staged plan to use the unique properties of the 21 cm “spin-flip” line from neutral hydrogen to probe our cosmic dawn, from the birth of the first stars and black holes through the full reionization of the primordial intergalactic medium (IGM). During this epoch, roughly 0.1–1 Gyr after the Big Bang, the neutral hydrogen that pervades the Universe following recombination is warmed, and then reionized by the first luminous sources. The Universe is transformed from one dominated by simple, linear evolution driven by gravity to an extraordinarily complex system with stars, black holes, and galaxies that dramatically change the state of baryons in the Universe through widespread heating and reionization. Direct observation of the large-scale structure of the primordial IGM, and its evolution with time, via the HI 21 cm line will have a profound impact on our understanding of the birth of the first galaxies and black holes, their influence on the surrounding gas, and cosmology.

HERA was ranked the “*top priority in the Radio, Millimeter, and Sub-millimeter category of recommended new facilities for mid-scale funding*” as part of the *New Worlds, New Horizons of Astronomy and Astrophysics* decadal survey (Committee for a Decadal Survey of A&A; NRC 2010; hereafter NWNH). The HERA roadmap initially envisioned a series of radio interferometers constructed throughout the decade. Phase I of this roadmap consisted of existing instruments — the Donald C. Backer Precision Array to Probe the Epoch of Reionization (PAPER) and the Murchison Widefield Array (MWA) — aimed at characterizing foregrounds and laying the groundwork for a statistical detection of the HI 21 cm signal through the power spectrum. A second-generation HERA instrument would measure the evolution of the power spectrum, revealing details of the astrophysics driving the birth and evolution of galaxies in the early Universe. A third-generation instrument would directly image structures throughout reionization.

With a fraction of the funding recommended for HERA Phase I in NWNH, the MWA and PAPER projects have made major strides in developing techniques to disentangle the reionization signal from the strong radio continuum foreground emission. These techniques, which are based on a new understanding of the interplay of foreground and instrumental systematics in the context of a

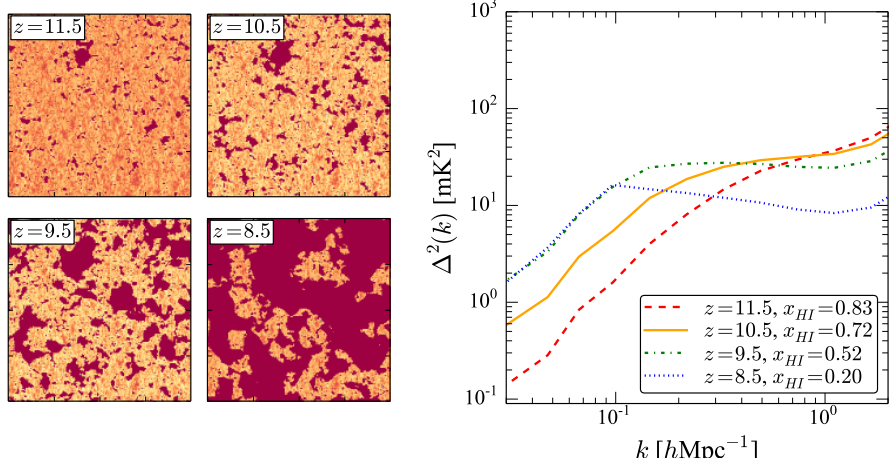


Fig. 2.— Left: Simulated 21 cm brightness temperature distributions spanning $\sim 280 \times 280 h^{-1} \text{Mpc}$ at $z = 11.5, 10.5, 9.5$, and 8.5 . Right: Corresponding evolution of the 21 cm power spectrum. HERA characterizes the power spectrum in detail, as well as providing images of the ionized bubbles (§2.1).

three-dimensional cosmological intensity-mapping experiment, have yielded a critical breakthrough. As discussed below, **we are now able to remove foregrounds to the limits of our sensitivity with these instruments**, and this is culminating in the first physically meaningful upper limits on the power spectrum of 21 cm emission from reionization (**Parsons et al. 2013**)¹

Using lessons learned from MWA and PAPER, we are now ready to build the instrument that delivers HERA-II science at a cost that is substantially below the $\sim \$60\text{M}$ envisioned in NWNH. The proposed HERA-331 experiment is based on a new 14 m diameter antenna element we have developed that is optimized for both sensitivity and minimizing foreground systematics. A compact hexagonal array of these elements improves sensitivity by nearly two orders of magnitude over the PAPER and MWA, and covers a wider frequency range (50 to 225 MHz). This design facilitates calibration, leverages proven foreground removal techniques, and supports multiple approaches to reionization studies. Construction proceeds in two stages, allowing both for technical improvements and the delivery of key science throughout the project period:

- HERA 127: A 127-element hexagonal array, deployed at the end of project year 2, measures the rise and fall of the 21 cm reionization power spectrum from $z = 7$ to 12 . These results tightly constrain the evolution of the IGM neutral fraction, determining the timing and duration of reionization.
- HERA 331: A 331-element hexagonal array, deployed at the end of project year 3, measures fluctuations in the 21 cm signal over a variety of spatial scales to determine the nature and distribution of the first galaxies that dominate cosmic reionization. HERA 331 extends precision power-spectrum observations back to the pre-reionization epoch ($z \sim 20$), when the first stars and black holes warm the primordial IGM. HERA-331 can also potentially image the largest structures in the primordial IGM — a task previously only considered possible with third-generation instruments.

This proposal is a self-contained package for delivering the core of HERA-II science, including telescope development, construction, observing, data analysis, and scientific products for each stage of the project. This approach minimizes risks associated with external funding contingencies while

¹Throughout the proposal, we have indicated work by members of the HERA collaboration in bold.

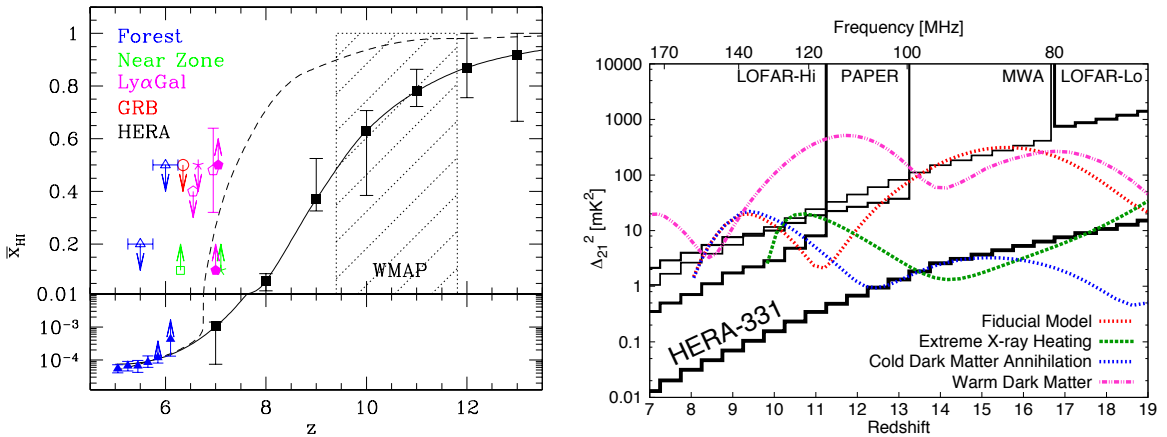


Fig. 3.— Left: Existing constraints on neutral fraction (x_{HI}) versus redshift (adapted from **Robertson et al. 2013**) along with a pair of fiducial reionization histories (black lines). The solid curve with error bars is a typical theoretical model of reionization consistent with WMAP measurements, while the dashed line is estimated from galaxy measurements at $z < 8$ and is consistent with most other constraints. The black markers with error bars show predicted HERA-331 constraints on the former model, demonstrating that we can distinguish allowed reionization histories at high confidence. Right: At lower frequencies, HERA probes pre-reionization physics at the end of the Dark Ages. Plotted are power spectrum amplitudes (at $k = 0.15h \text{ Mpc}^{-1}$) for various IGM heating models (Mesinger et al. 2013), with predicted sensitivities.

encouraging collaborators to leverage resources for augmenting HERA’s science.

2. Scientific Justification and Intellectual Merit

Our *cosmic dawn*, the period beginning with the birth of the first stars and culminating with the full reionization of the IGM ~ 1 Gyr later, represents one of the last unexplored phases in cosmic history. This period is rich in both astrophysical and cosmological phenomena. The characteristics of the IGM depend on the cosmic density field, the first galaxies (e.g., their typical masses and clustering), their constituents (e.g., exotic Pop. III stars, more normal stars, stellar remnants, or supermassive black holes), their ultraviolet luminosities (which affect the IGM ionization and thermal states), the efficiency and abundance of X-ray sources (which affect IGM temperature), and cosmological effects like the relative velocities of baryons and dark matter. Exploring these early structures and their interplay with their environment was one of the top three “*priority science objectives chosen by the [NWNH] survey committee for the decade 2012-2021*.”

The study of the formation of the first galaxies and their influence on the primordial IGM is among the highest priorities in modern astronomy and a primary driver for many future large telescopes. Recent measurements from the *Hubble Space Telescope* have pinned down the bright end of the galaxy luminosity function at $z \lesssim 8$ (Bouwens et al. 2010; Schenker et al. 2013) and have detected a few sources at even greater distances (Ellis et al. 2013; Oesch et al. 2013). Still, this known population falls well short of the requirements to reionize the universe, driving us to deeper observations with, e.g., JWST and ALMA, to reveal the fainter end of the luminosity function. In parallel, a number of indirect techniques have constrained the evolution of the neutral fraction with redshift, although predominantly at the end of reionization. Figure 3 summarizes these observations, including:

- Measurements of the optical depth to reionization based on CMB temperature fluctuations (Planck Collaboration et al. 2013) and large scale polarization anisotropies (Page et al. 2007)
- Observations of resonant scattering of Ly α by the neutral IGM toward distant quasars (the

‘Gunn-Peterson’ effect) (Fan et al. 2006).

- The demographics of Ly α emitting galaxies (Schenker et al. 2013; Treu et al. 2013; Faisst et al. 2014).
- The Ly α absorption profile toward the most distant quasar ($z = 7.1$) (Bolton et al. 2011).
- Secondary temperature fluctuations generated by the kinetic Sunyaev-Zel’dovich effect (Zahn et al. 2012; Mesinger et al. 2012).

Although the existing limits are weak and model-dependent, there is substantial tension between the CMB measurements — which suggest that the bulk of reionization occurred at $z \sim 10$ (within the hatched box in Figure 3) — and others measurements. This suggests (albeit at low confidence) that reionization was still substantially neutral as late as $z \sim 7$ (with the HI ionization fraction as high as $x_{HI} \sim 0.5$). The two curves in the left panel of Figure 3 illustrate this tension: the solid curve is consistent with the CMB measurements and follows simple assumptions about galaxy formation, while the dashed curve is extrapolated from galaxy observations (Robertson et al. 2013).

Unfortunately, existing methods are unable to resolve this tension. In particular: (1) probes using the Ly α line can study only the tail-end of reionization, due to the extreme optical depth of that transition; (2) inferences from galaxy populations require strong assumptions regarding stellar populations, galaxy structure and evolution, and undetected sources; and (3) the CMB provides only an integral measure of ionization back to recombination.

The 21 cm “spin-flip” transition of neutral hydrogen has been recognized as potentially the most powerful probe of the cosmic dawn (Morales and Wyithe 2010; Furlanetto et al. 2006), as emphasized in NWNH: “*The panel concluded that to explore the discovery area of the epoch of reionization, it is most important to develop new capabilities to observe redshifted 21 cm HI emission, building on the legacy of current projects and increasing sensitivity and spatial resolution to characterize the topology of the gas at reionization.*” Because our Universe was almost entirely neutral before reionization, the HI 21 cm line provides a direct method to image the evolution of the primordial IGM, opening a unique window into the complex astrophysical interplay between the first luminous structures and their surroundings. Moreover, because of the cosmological redshift, we can associate the signal at each observed frequency with a particular emission time (or distance) and reconstruct a complete three-dimensional picture of the time evolution of large scale structure during this key epoch in observational cosmology.

Decades of effort have gone into modeling the complex astrophysics of reionization (e.g. Shapiro and Giroux 1987; Haiman and Loeb 1997; Furlanetto et al. 2004; Santos et al. 2010). Figure 2 shows a simulation of the expected evolution of the HI 21 cm signal during reionization (Mesinger and Furlanetto 2007). Fluctuations in the signal initially rise above those expected from the cosmic density field due to the growth of ionized bubbles on a characteristic scale of several arcmin. This scale is set by the clustering of early galaxy formation, as well as by propagation effects through the IGM. The signal then declines as the IGM becomes fully ionized. These theoretical models of the reionization process are sophisticated and appear to be well-understood, but they are not predictive tools. Instead, they provide a mapping between the largely unknown galaxy populations and observables like the 21 cm transition. As such, the key questions about the cosmic dawn era remain poorly understood. When did reionization occur, and over what timescale? What objects dominated the process, and how were they distributed? What role did stellar (and other)

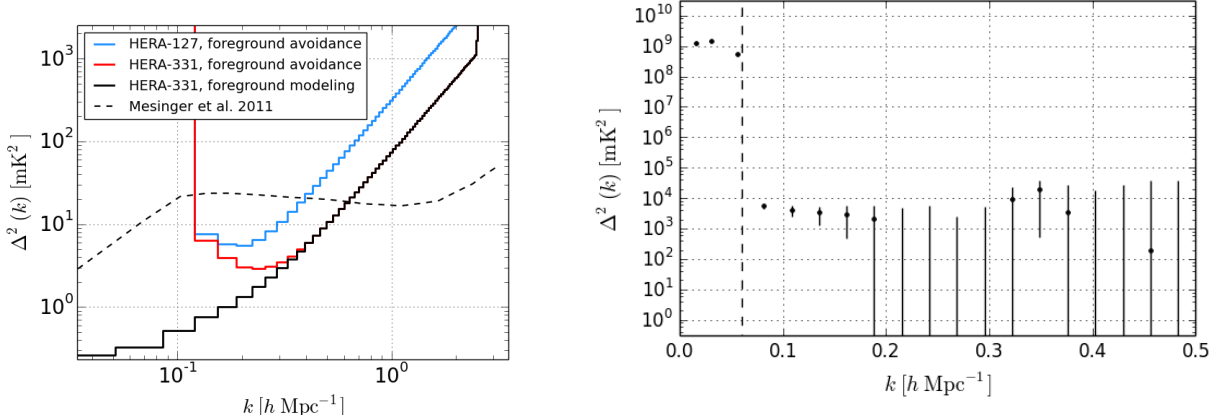


Fig. 4.— Left: HERA’s power-spectrum sensitivity (solid) relative to a fiducial ionization model (dotted line; $x_{\text{HI}} = 0.37$, $z = 9.0$). Sensitivities reflect staged array size and improving analysis software that expands the range of modes free of foreground systematics. Right: The current best upper limit on the 21 cm reionization power spectrum, obtained with a 32-element PAPER deployment (Parsons et al. 2013). Note the sharp drop in spectrally-smooth foreground power at the horizon, indicated by the dashed line (c.f. Figure 9). The upper limits at $k \sim 0.2 \text{ hMpc}^{-1}$ constrain the brightness temperature of the IGM at $z \sim 8$, showing a departure from adiabatic cooling presumed to be indicative of X-ray heating.

feedback mechanisms play during this era? *HERA provides the key measurements needed to advance our understanding of early galaxy formation and cosmic reionization.*

2.1. Science From Reionization and Cosmic Dawn

As a high-sensitivity instrument with broad frequency coverage, HERA can paint an uninterrupted picture of the IGM through reionization and into the era of the cosmic dawn. This capability leverages the coupling of 21 cm emission to radiation fields generated by the first galaxies (in the UV and X-ray) to transform our understanding of the very first galaxies. Figure 3 illustrates how HERA determines the ionization history of our universe much more precisely, and over a wider redshift range, than is possible with other existing techniques, easily distinguishing the pair of (currently allowed) ionization histories shown in the diagram. Because these integrated radiation fields are otherwise inaccessible, these measurements propel us beyond characterizing the timing and duration of reionization and into a regime of answering the detailed astrophysical questions described in the previous paragraph. At higher redshifts ($z \sim 15$ to 20), the sensitivity of the 21 cm line to the IGM temperature (set partly by X-ray heating) provides a unique probe of black holes and other X-ray sources during this early epoch – an era that may be otherwise untestable, even with JWST.

Power Spectrum Detection. A season of observing with HERA-127 yields high-significance constraints on the 21 cm power spectrum across a wide range of wavenumbers and redshifts (Pober et al. 2014). Figure 4 shows a $z = 9$ power spectrum modeled by the 21cmFAST software (Mesinger et al. 2011), along with 2σ HERA sensitivities. Using a proven “foreground avoidance” approach (see §3.1) we find that HERA-127 achieves a $> 10\sigma$ detection over a broad range of redshifts. Subsequent observing with HERA-331 boosts this to $> 25\sigma$, as described in Table 1. With detailed foreground modeling techniques developed for the MWA, the overall significance rises to 90σ , along with new access to smaller k modes and therefore qualitatively different physics.

Constraining Model Parameters. Power spectrum measurements with HERA-331 are sensitive enough to place strict constraints on theoretical models of reionization and even to test the

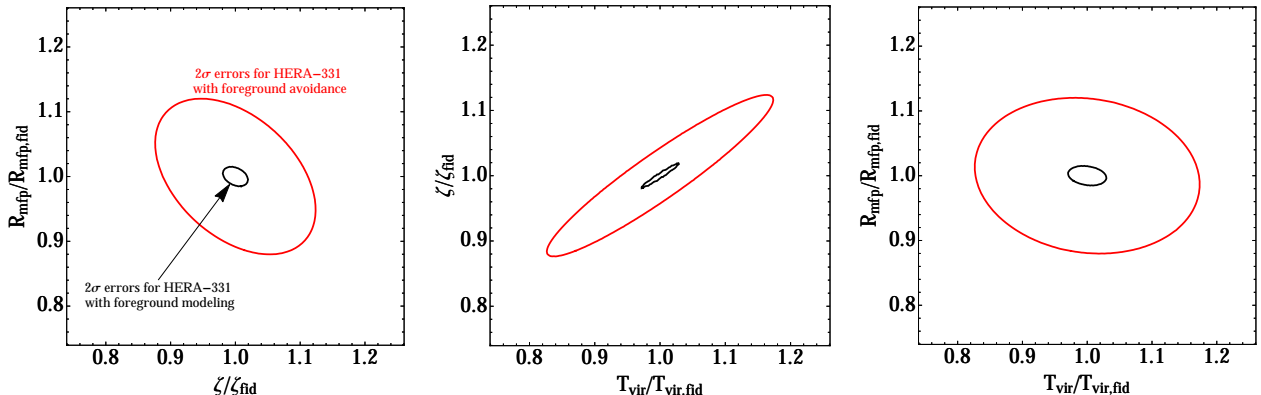


Fig. 5.— Pairwise 2σ error ellipses for T_{vir} , ζ , and R_{mfp} , in each case divided by their fiducial values. HERA-331 projections using existing foreground avoidance techniques are shown in red, while projections using more advanced foreground modeling techniques are shown in black. The former represent $\sim 5\%$ constraints, while the latter represent $\sim 1\%$ constraints.

fundamental assumptions of those models. Within the standard framework, three terms determine the major features of the power spectrum: ζ , the efficiency at which galaxies release ionizing photons into the IGM; T_{vir} , the minimum virial temperature of halos that produce ionizing photons; and R_{mfp} , the mean free path of ionizing photons in the IGM (determined by the abundance of optically thick clumps). Existing observations limit the values of these parameters to within an order-of-magnitude at best. Figure 5 shows that we expect HERA-331 power spectrum observations to constrain them to better than 5% using proven foreground avoidance techniques, with even stronger constraints from explicit foreground modeling (Pober et al. 2014).

Imaging HI. With a nearly completely sampled aperture over 300 m across, HERA has the collecting area of Arecibo, but with $500\times$ the survey speed and sufficiently high sensitivity to image reionization directly. After 100 hours on a single field (achievable in 200 nights), HERA reaches a surface brightness sensitivity of $50 \mu\text{Jy}/\text{beam}$ (synthesized beam FWHM $\sim 24'$) compared to the brightness temperature fluctuations of up to $400 \mu\text{Jy}/\text{beam}$ in typical reionization models. In Figure 6 we demonstrate the imaging sensitivity arising from a foreground avoidance scheme, assuming a conservative 1 MHz of effective bandwidth, corresponding to 12 Mpc along the line of sight. It remains to be seen whether foregrounds can be as robustly mitigated for imaging as they can be for power spectrum measurements, but from the standpoint of sensitivity alone, HERA is capable of detecting the brightest structures at $z = 8$ with $\text{SNR} > 10$.

Pre-Reionization Heating. Pending the development of a wider observing band, HERA has the sensitivity to push the redshift frontier of current-generation 21 cm instruments to the pre-reionization era ($z \sim 20$). In standard theoretical models, this allows us to measure an earlier peak in the power spectrum generated during the era of X-ray heating (most likely sourced by stellar remnants). These scenarios encompass a wide range of possibilities for IGM heating, as shown in Figure 3 (see Mesinger et al. 2013) with HERA’s sensitivity overlaid. HERA’s constraints in this epoch can determine the rate and density of massive black hole formation in the early universe (Pritchard and Loeb 2010), or identify contributions by exotic heating sources like dark-matter annihilation or the existence of warm dark matter. In some scenarios, HERA is also sensitive to the velocity streaming between baryonic matter and the dark matter halos and its effect on early structure formation and the onset of Ly α emission (Visbal et al. 2012). HERA’s

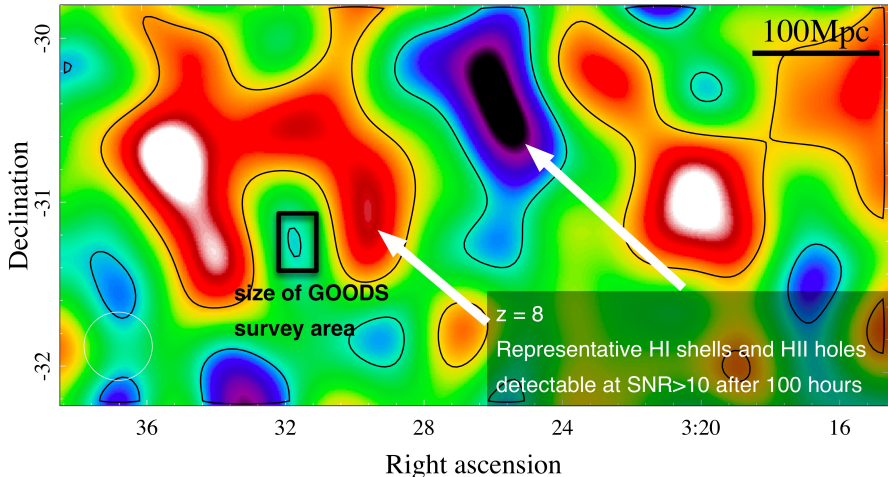


Fig. 6.— With sensitivity concentrated at the largest scales and a survey area of 2600 square degrees, HERA-331 has the sensitivity to directly image HI during reionization. Contours indicate 10σ detections of a simulated reionization field (McQuinn et al. 2007) with a 100-hour observation.

development activities with regard to lower-frequency performance are aimed at taking advantage of the pre-reionization era as an unparalleled testbed for both astrophysics and cosmology.

Cross-Correlations. The ability of HERA to image enables an exciting range of cross-correlation science. HERA HI images can reveal the large-scale reionization environment for pointed ALMA and JWST observations and other deep near-IR surveys (Lidz et al. 2009). Knowing whether an observed galaxy is in a region that was previously reionized (such as the center of a large HII bubble), recently reionized (the edge of an HII bubble), or is forming from pristine HI provides important contextual information on early galaxy formation and especially feedback. HI images can also be cross-correlated with other diffuse tracers of large scale structure, including intensity mapping of molecular CO (Lidz et al. 2011), atomic CII (Gong et al. 2011), and HI Ly α (Silva et al. 2013) lines. These studies trace the large scale galaxy distribution – the sources of reionization – and cross-correlation with IGM images can break degeneracies within both data sets as well as provide clean measurements of the underlying signal (because independent systematics cancel out in the cross-correlation). Prototypes of such experiments may be operating contemporaneously with HERA.

3. Achievements Under Prior NSF Support

The HERA project team consists of PIs and technical leaders from four NSF-funded projects targeting the 21 cm signal at high redshifts:

- PAPER (NSF grants #1129258, #0804508, #0607838, and #0505354) has followed a staged development approach, maintaining a technical development array in Green Bank, WV, and a science array in the Square Kilometre Array (SKA) radio quiet zone in the Karoo, South Africa. Starting with a 16-element array in 2009 in the Karoo, PAPER has doubled its size annually for four years running. Under the current grant, “*Collaborative Research: Precision Array for Probing the Epoch of Reionization (PAPER)*” (#1129258, \$2,629,198, 09/11 – 08/15), this has culminated in the promised 128-element array (Figure 7; Parsons et al. 2012a), delivered on schedule with extra cross-polarization functionality. PAPER pioneered the use of redundant antenna configurations for power-spectrum measurements, the use of drift-scanning elements, a scalable correlator architecture, and real-time 40-fold data com-

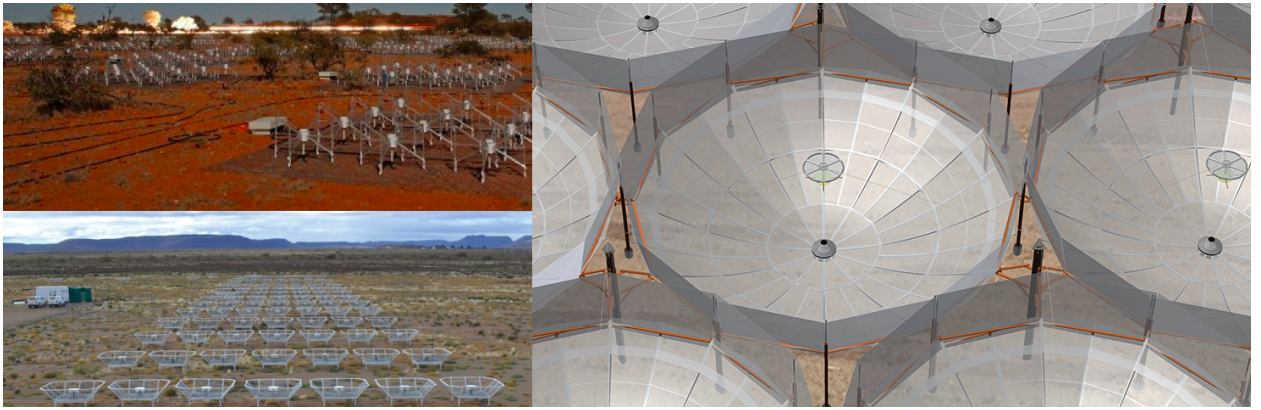


Fig. 7.— The MWA (top left) and PAPER (bottom left) arrays, each currently deployed with 128 elements. The 14-m HERA element (right) dramatically improves sensitivity while constraining the path length and amplitude of reflections to ensure that foreground isolation is not substantially degraded.

precision based on delay/delay-rate filtering. PAPER pioneered the delay-spectrum foreground avoidance technique (**Parsons et al. 2012b**), and applied it to observations (Fig. 4; **Parsons et al. 2013**). The resulting power spectrum places the best upper limit on reionization by almost two orders of magnitude in mK², and was used to show that the IGM must have been heated prior to reionization — presumably by emission from high-mass X-ray binaries.

- The MWA (NSF grants #0457585, #082132, #1109257), located at the future SKA-low site in Western Australia, was developed as a large international collaboration. It consists of 128 digitally steerable antenna tiles (Fig. 7, upper left; **Tingay et al. 2013**), arranged in an imaging configuration, and operating from 80 to 300 MHz. The US MWA team is a world leader in the application of image-based modeling techniques (Fig. 9, right) to foreground subtraction (e.g. **Hazelton et al. 2013; Morales et al. 2006**). Recent MWA observations have demonstrated the subtraction of foregrounds to the thermal noise limit in regions dominated by systematics using delay-spectrum analysis techniques (Fig. 9, left). Such techniques potentially expand the number of modes available to HERA for measuring the 21 cm reionization signal, and can suppress polarized foregrounds that may enter delay-spectrum measurements near the level of the reionization signal (**Moore et al. 2013**).
- MITEoR (NSF grants #1105835, #0908848) is a 64-element array examining novel cross-correlation and calibration techniques for 21 cm reionization experiments. While spatial-FFT cross-correlation techniques remain under development, MITEoR brings critical expertise in redundancy-based calibration and quadratic power-spectrum estimation techniques.
- LEDA (NSF grant #1106045) is a 256-element array targeting the global 21 cm reionization signal. Werthimer and Greenhill collaboratively pioneered the application of graphics processing units (GPUs) in digital correlators. This technology was adopted in recent PAPER deployments, and is applied to HERA’s correlator and data-compression systems.

Other projects involving HERA team members that have undertaken significant hardware development and completed major deployments include the EDGES experiment (NSF grants #1207761, #0905990), the Center for Astronomy Signal Processing and Electronics Research (CASPER; NSF grant #0906040), the Advanced Multibeam Spectrometer for the GBT (NSF grant #1006509), and numerous other efforts. On the theory side, “Theoretical Models of Helium Reionization” (NSF grant #0829737, #0607470) created and publicly distributed the semi-numeric reionization code,

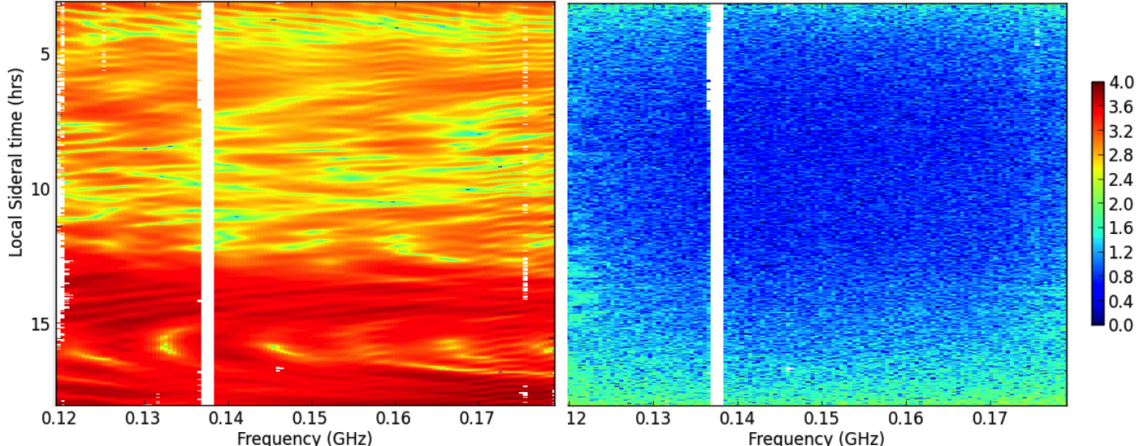


Fig. 8.— Waterfall plots illustrating PAPER visibilities measured on a 30-m baseline before (left) and after (right) the application of a delay filter that eliminates foreground emission within the wedge. Color scale indicates amplitude in $\log_{10}(\text{Jy})$. This filter suppresses foreground systematics by > 4 orders of magnitude, leaving residuals demonstrably noise-dominated while preserving the reionization signal.

DexM. The broader impacts of these efforts are discussed in §5.2.

These projects have a strong publication record of ground-breaking research in peer-reviewed literature, and bring to HERA mature hardware designs, software pipelines, and powerful scientific and analysis frameworks. HERA’s leadership also brings substantial experience collaborating internationally, managing the design, development, testing, and integration of complex systems, adhering to project timelines and budgets, and setting incremental development and deployment plans that ensure that progress is made on a predictable schedule, with time to adapt to contingencies.

3.1. Lessons for HERA

The key challenge of 21 cm reionization experiments is balancing the collecting area needed to detect the faint reionization signal with the precision needed to suppress foregrounds that are ~ 5 orders of magnitude brighter (de Oliveira-Costa et al. 2008; Jelić et al. 2008). Previously, it was assumed that careful calibration and image-based model subtraction would be the keys to overcoming these foregrounds (Liu et al. 2008; Bowman et al. 2009; Harker et al. 2009). While such efforts are being actively pursued and are likely to be important to the field in the future, it has become clear that the community underestimated the challenges associated with this approach. The major breakthrough for 21 cm reionization experiments — what enables us to propose HERA now — is the discovery of how instrumentation and analysis can instead exploit the spectral smoothness of foregrounds to open up a window for accessing the reionization signal. As illustrated in Figure 8, these advances have been used to suppress foreground emission by at least 4 orders of magnitude in PAPER observations, with results that begin ruling out certain reionization scenarios (Parsons et al. 2013).

For redshifted (21 cm) line emission, each observing frequency maps to a line-of-sight distance. Hence, measurements as a function of frequency and angle enable 21 cm reionization experiments to map a cosmological volume $\{x, y, z\}$ in comoving Mpc. For power-spectrum measurements, this observed volume is Fourier transformed into a wavenumber cube $\mathbf{k} \equiv \{k_x, k_y, k_z\}$, where $k_\perp \equiv \{k_x, k_y\}$ represents angular Fourier modes that are directly related to the (u, v) modes sampled by baselines of an interferometer, and $k_\parallel \equiv k_z$ is a line-of-sight wavenumber. The expected statistical isotropy of the signal allows measurements in k -space to be squared and averaged in shells to

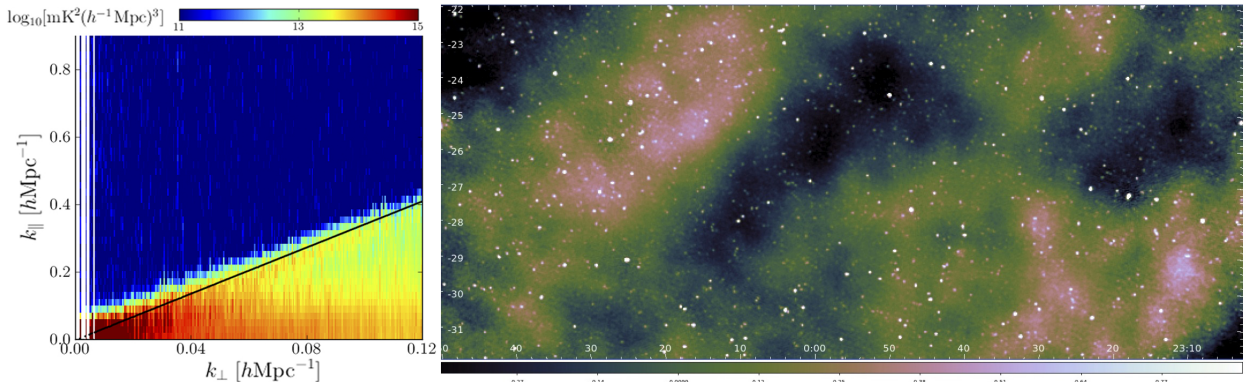


Fig. 9.— Left: PAPER observations (**Pober et al. 2013**) show foreground contamination in line-of-sight k_{\parallel} vs. angular k_{\perp} to be confined to a bright wedge, leaving other modes thermal-noise limited. Right: A $\sim 10^\circ \times 25^\circ$ image of foregrounds by the MWA illustrates methods that provide key capabilities for reducing polarization leakage and foreground systematics within the wedge for HERA observations.

produce the spherical power spectrum shown in Figure 4.

Rather than inverting interferometric measurements to make images, a powerful new approach has been developed and tested by the PAPER and MWA teams that instead directly Fourier transforms each baseline separately along the frequency axis, effectively producing a wavenumber cube while still handling interferometric chromaticity on a per-baseline basis. Because of the way smooth-spectrum foregrounds interact with baselines of different lengths, this flexibility to handle baselines separately is critical. Through a concerted theoretical and observational campaign by PAPER and the MWA (**Morales et al. 2012; Parsons et al. 2012b; Vedantham et al. 2012; Datta et al. 2010; Hazelton et al. 2013; Pober et al. 2013; Parsons et al. 2013; Dillon et al. 2013b**), we now understand that foreground contamination is confined to a ‘wedge’ in k_{\parallel} vs. k_{\perp} , as demonstrated by the PAPER observations in Figure 9. Because the k_{\parallel} direction (obtained by Fourier-transforming along the frequency axis) is effectively an “inverse frequency” (e.g. time delay), the form of this wedge can be understood analytically as arising from the relative delay between sky signals entering each antenna in an interferometric baseline from different directions. (Faraday-rotated emission from extragalactic sources may introduce additional foreground emission outside the wedge (Labropoulos et al. 2009; Jelić et al. 2010; **Moore et al. 2013**); we discuss plans for mitigating polarization leakage and removing this source of contamination in the Analysis/Science Risk section of the Project Management Plan.)

Our new understanding of the foreground wedge has two powerful consequences. Firstly, as illustrated in Figure 8, the foreground wedge can be removed with a baseline-dependent filter that eliminates emission within a well-defined range of spectral smoothness. This filter directly suppresses foregrounds by at least 4 orders of magnitude, and leaves the region above the wedge free from foreground emission — a window through which we can observe the reionization signal. Secondly, by understanding signal delay as the mechanism that gives rise to the wedge, it is now possible, for the first time, to map foreground removal requirements to the precise instrumental characteristics that are required. The most direct instrumental constraint comes from the fact that, to access \mathbf{k} -modes in the range $0.1 < k < 0.2 h \text{ Mpc}^{-1}$ where 21 cm reionization experiments can be most sensitive, **the signal delay between antennas contributing to this measurement cannot exceed 120 ns**. As discussed in §4, this constraint can (and must) be incorporated into the fundamental design of any future 21 cm reionization instrument.

Instrument	Collecting Area (m ²)	Foreground avoidance	Foreground modeling
PAPER	528	1.93	8.86
MWA	896	2.46	6.40
LOFAR NL Core	35,762	2.76	17.37
HERA-127	19,500	10.88	35.65
HERA-331	50,900	25.44	87.20
SKA1 Low Core	833,190	97.92	284.85

Table 1: Power spectrum signal-to-noise (“number of sigmas”) at $z = 9.5$ for various instruments, adapted from **Pober et al. (2014)**. By leveraging a filled, redundant configuration of dishes with high collecting area, HERA-331 allows high-significance power spectrum measurements using current foreground avoidance techniques, with further enhancements possible with likely advances in foreground modeling.

4. HERA Project Design

We have achieved a pivotal new understanding of how instrumental characteristics give rise to the wedge of emission shown in Figure 9. Furthermore, we have measurements that prove the efficacy, to the sensitivity limits of current instruments, of projecting out foreground-dominated wavemodes within the wedge. The HI cosmology community is now in a position to define the top-level instrument requirements that ensure foregrounds remain bounded within the wedge, and to specify the sensitivity needed to obtain high-significance detections of the 21 cm reionization power spectrum under the conservative assumption that all foreground-dominated wavemodes within the wedge must be projected out of our measurements. As summarized in Table 1 (see **Pober et al. 2014** for more details), based on these assumptions, current instruments are likely to achieve, at best, only marginal detections of power from reionization.

This proposal targets two arrays: a 127-element array that borrows heavily from components of the PAPER experiment, and an upgraded 331-element array that incorporates several performance optimizations. These arrays are developed over four years (see Fig. 10 and the Project Management Plan for details), with recurring cycles of development, testing, review, deployment, commissioning, and observation. As listed in Table 1, the specifications of HERA-127 and HERA-331 have been set to meet precisely the requirements for obtaining, respectively, a 10σ detection of the 21 cm reionization signal across a broad range of redshifts, and a 25σ detection of the power spectrum of fluctuations in the 21 cm signal capable of determining the nature and distribution of the first galaxies that dominate cosmic reionization. As discussed in §3.1, these science requirements translate directly into requirements for signal delay and collecting area that, when combined with a cost minimization requirement, tightly bound the HERA design. The basic parameters are given in Table 2.

4.1. Instrument Design

As shown in Figure 11, the HERA instrument has a straightforward signal path from antenna elements with active feeds, to nodes that digitize and aggregate signals onto an optical network, and on to a processing building where signals are correlated and data are stored, compressed, and shipped to a computing cluster located at U. Pennsylvania (UPenn).

4.1.1. Antenna Element

The novel design of HERA’s antenna element (Fig. 7, right panel) represents a critical advance that enables HERA to achieve its science goals. This 14-m fixed zenith-pointing parabolic dish

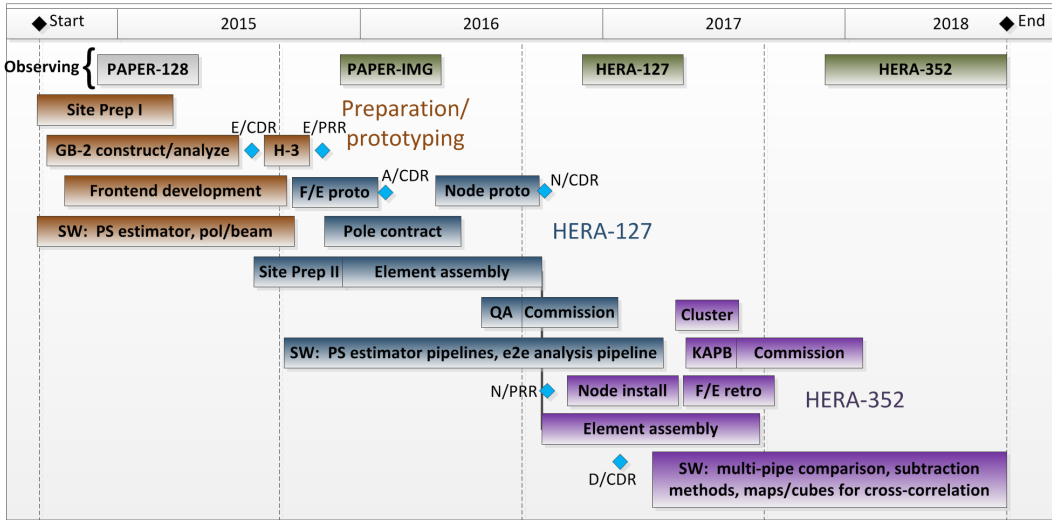


Fig. 10.— Project timeline showing development phases (orange/blue/purple) and observing periods (green).

yields more than 10 times the sensitivity of an MWA tile (and more than 20 times that of a PAPER element), but does so without substantially degrading our ability to isolate and remove foreground emission on the basis of spectral smoothness. As described above, this is done by limiting the timescale of signal delays and reflections to under 120 ns.

Since the time it takes radio emission to propagate between adjacent antennas represents a significant portion of this time budget, HERA elements must be placed close together. Recent work characterizing foregrounds suggests that antenna separations of $8\lambda \approx 15\text{m}$ are well-behaved to current limits (Pober et al. 2013; Parsons et al. 2013). This influences our choice of a 14-m dish diameter, which incurs 42 ns of signal delay between adjacent antennas. The focal height (4.5 m) derives from the illumination pattern of the prime-focus feed and the fact that reflections between the feed and the element can introduce additional signal delay. Additional measures, such as a splash cone underneath the feed, screens that isolate feeds from one another, and non-metallic cabling and poles for supporting the feeds, are all aimed at minimizing the potential for additional sources of signal reflections. The total signal delay associated with the HERA dish design is estimated at 83 ns, leaving headroom for reflections arising in the analog signal path.

Cost is another design constraint, including the price of construction materials, assembly in a remote area, and maintenance over the operational lifetime of the array. Care has been taken to select robust and inexpensive construction materials (PVC, concrete, utility poles, 0.25" wire cloth) and an assembly methodology that delivers the required positional accuracy of 10 cm and surface accuracy of 2 cm given standard expertise in construction practices for the subcontracted teams that set the poles and construct the elements in the field. Given the sensitivity and signal delay requirements, the size of HERA dishes optimizes a global costing curve that includes the costs of the elements, the signal path, correlation, data storage, and processing.

A first prototype of the HERA dish is nearly completely constructed. In this proposal, UC Berkeley and NRAO lead the incorporation of lessons from the construction process and reflectometry tests into the design. Two further prototype elements are constructed in the first year alongside the existing PAPER array in Green Bank, WV, for on-sky measurements of the beam pattern and spectral response. These measurements are coupled with full electromagnetic modeling to test and refine the element design prior to a Critical Design Review at the end of the first project.

Parameter	Design	Performance
Element diameter / FoV	14 m	9°
Min baseline length / largest scale	14.6 m	7.8°
Max core baseline length / synthesized beam	306.6 m	24'
Max outrigger baseline length	1066.5 m	9'
Frequency / redshift range	50 - 250 MHz digitized 70 - 230 MHz useable 100 MHz correlated	19.2 - 5.2
Spectral channel width	97.7 kHz	
System temperature / sensitivity	$100 + 120(\nu/150 \text{ MHz})^{-2.55} \text{ K}$	$50 \mu\text{Jy beam}^{-1} \sqrt{\text{hour}}$

Table 2: HERA-331 basic parameters. Design parameters are connected to the derived instrument performance at 150 MHz.

year. Three revised elements are then constructed in South Africa, involving lead members of the construction subcontract teams for a Project Readiness Review.

4.1.2. Array Configuration

For HERA-127 and HERA-331, elements are arranged in a compact hexagonal grid. This configuration minimizes antenna separation, which is critical for meeting the science requirements for foreground isolation, and produces a highly redundant sampling of the uv plane. As described in §3.1, redundant configurations have been employed by PAPER to boost sensitivity (**Parsons et al. 2012a**), with the added benefit that they greatly facilitate fast and accurate calibration (**Liu et al. 2010; Parsons et al. 2013**). Placing HERA elements in a grid allows certain construction components to be re-used between antennas, reducing cost and improving the accuracy of element placement. HERA-331 is a build-out of HERA-127 from the eastern edge.

The HERA-331 core has excellent imaging capability that can be leveraged for developing foreground suppression techniques to improve access to the 21 cm reionization signal (Fig. 4, black). This capability is augmented with 21 outrigger elements. These outriggers combine with the dense core to generate a fully sampled uv plane out to 400λ . While outriggers on the southern half of the array are placed in alignment with the hexagonal grid in the core, elements on the northern side are shifted off-grid to sample the uv plane at sub-aperture scales. This sampling strategy helps eliminate grating lobes in the synthesized beam and provides information for calibrating and correcting direction-dependent antenna responses. This capability may be used to match polarization beams and minimize polarization leakage.

4.1.3. Analog Signal Path

HERA’s analog signal path inherits directly from PAPER. In keeping with a philosophy of incremental change, HERA-127 reuses the tested and commissioned feed, LNA, cables, and post-amplifier gain modules (Fig. 13, left and center) that are currently being used to good effect in PAPER-128 (**Parsons et al. 2010**). Existing PAPER feeds are attached to new reflector screens that are suspended over the elements, but otherwise remain unmodified. A parallel development effort in NRAO aims to improve the feed response below 100 MHz and to improve the match between polarization beams in the feed-element system. Additional minor modifications to the analog signal path include transitioning from a 75Ω to a shorter 50Ω cabling system and replacing 100–200 MHz bandpass filters with 50–250 MHz equivalents. This wider analog bandwidth is used in HERA analysis to improve the extrapolation of smooth foreground emission over a broader range, and to

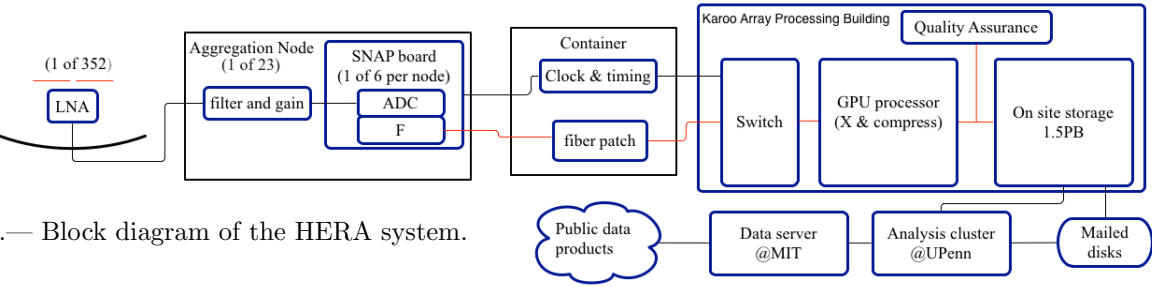


Fig. 11.— Block diagram of the HERA system.

explore HERA’s capability as a Dark-Ages science instrument. After a Critical Design Review, the results of these development efforts are incorporated in the transition to the HERA-331 system.

4.1.4. Digital System

Although correlators have historically been one of the most complex, expensive, and risky aspects of developing a radio interferometer, this is no longer the case. CASPER (**Parsons et al. 2006**) open-sourced the development of digital signal processing engines for astronomy and now has world-wide participation, with over 500 members at 73 institutions, and five generations of hardware (Fig. 14). On a modest budget, PAPER has applied CASPER technology to develop and deploy new correlators annually for five years running, each quadrupling the computational capacity of its predecessor. Led at UC Berkeley’s Radio Astronomy Lab (RAL), HERA efforts continue this incremental development cycle, following a packet-switched correlator architecture (**Parsons et al. 2008**) that has been extended in recent PAPER and LEDA deployments (Fig. 13, right) to leverage the computing strengths of both FPGAs and GPUs (Clark et al. 2011).

While HERA-127 uses the existing PAPER correlator directly, this correlator architecture evolves for HERA-331. As discussed in previous sections, HERA’s science requirements dictate a maximum analog signal path-length. As a consequence, digitization needs to happen close to the antenna elements in the field. This specification, along with a growing need for modularity to scale with the number of parallel signal paths, leads HERA to adopt a node-based architecture for amplification, digitization, channelization, and digital transmission in the field that builds on HERA’s MWA heritage. This architecture is merged with PAPER’s clean architecture for real-sampling and channelizing the entire analog passband at once, packetizing the data into 10 Gb Ethernet format, and relying on commercial switches to perform the frequency/antenna corner-turn that FX correlator architectures require.

Node. HERA-331 employs RFI-tight node enclosures that each contain the final gain and digitization stages for signals from 18 antennas, along with power supplies, cooling, and a small server for monitor/control. As part of HERA development, a new board called the Smart Network ADC Processor (SNAP) board is incorporated into the CASPER suite of hardware and firmware. This inexpensive board was co-designed by UC Berkeley and NRAO to be both the digitizer and F-engine in HERA’s FX correlator architecture, and is currently in layout at NRAO. Each SNAP board digitizes and channelizes a 50–250 MHz band for 6 input signals (3 antennas, dual-polarization). A 100-MHz band of selectable channels is transmitted over optical fiber to a central container (see below), and on to the Karoo Array Processing Building (KAPB). The development and integration of the SNAP design and the node system is led at UC Berkeley and after a Critical Design Review, is fabricated under subcontracts to industry partners in the third project year and deployed as part

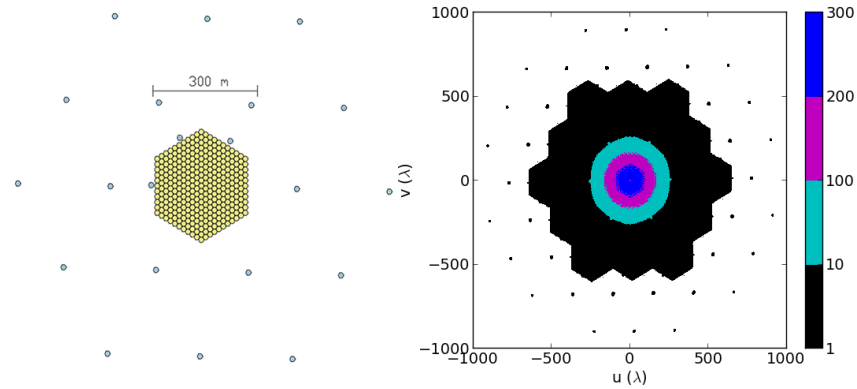


Fig. 12.— Left: Configuration of HERA-331, with 331 dishes in a maximally-dense hexagonal core (yellow) and 21 outrigger dishes (blue). Right: The resulting uv -coverage is fully-sampled to $\sim 400\lambda$

of the HERA-331 system. Development activities under this proposal include porting the CASPER toolflow to the SNAP board, designing and testing the FPGA firmware, integrating and testing all components in the node subsystem, and providing a monitor/control access interface. If time allows, optional development may include doubling the transmitted bandwidth.

Central Container. HERA’s central container houses two significant subsystems adjacent to the array. The first is a timing subsystem that maintains a GPS-disciplined oscillator and distributes timing signals (the sampling clock and 1PPS synchronization) to the nodes. The second subsystem is a passive fiber optic patch panel that couples the optical network from the nodes into the 192-filament optical fiber bundle that connects to the KAPB.

Karoo Array Processing Building (KAPB). The KAPB is currently in advanced stages of construction for MeerKAT, and houses the switch and processors that complete the HERA correlator system. The fiber optic bundle that enters the KAPB patches into local fiber optic cables that each terminate in optical transceivers that plug into a 240-port 10 GbE switch. Such switches, while large, are readily available commercially today. Also connected to this switch are 30 servers, each hosting two dual-GPU graphics cards and two dual 10 GbE network interface cards, which implement the cross-multiplication (X-Engine) component of the correlator during observations. This estimate for the number of X-Engine servers is extrapolated from current GPU servers deployed on PAPER, assuming no improvement in bus speeds for transferring data into the GPU cores, but assuming that the computational capacity of such GPU cores doubles according to Moore’s Law prior to the purchase of these servers in the third year of the project. Output data from the correlator are written to the data storage system described in the following section.

4.1.5. Data Storage, Compression, Transfer, and Computing

HERA’s data management system is responsible for recording raw data from the correlator, compressing that data in real-time, applying routine calibration and analysis pipelines, and transferring data products to a high-performance computing cluster at UPenn. UPenn leads the procurement and deployment of three data storage systems:

- a 1.5 PB system deployed in the KAPB for archiving all 1.2 PB of raw data and 60 TB of compressed data,
- 6 network attached storage (NAS) units plus 2 125 TB RAID array units that are used to ship compressed data products to the US, and
- a permanent 250 TB system at UPenn associated with a computing cluster that holds com-

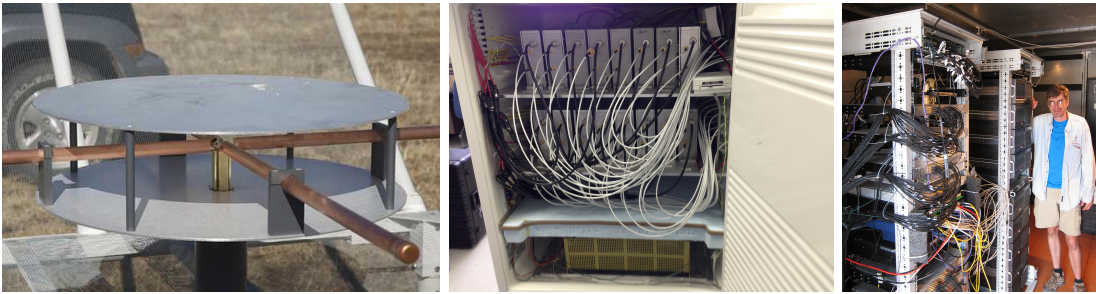


Fig. 13.— Existing components re-used in the HERA design include: the PAPER dipole antenna (left), receivers in a node module (center), and the 128-element correlator deployed in the Karoo (right).

pressed data products and serves as the analysis engine for HERA collaborators. This effort leverages existing infrastructure at UPenn, with support for the expansion of the data storage and for upgrading to a 30-node computing cluster. This cluster supports the bulk of the analysis by HERA collaborators (see §4.3) that requires access to the full set of HERA observations.

The data compression scheme at the heart of the data management system has been implemented for PAPER (**Parsons et al. 2013**, Appendix A), and is applied to HERA visibilities to reduce data volume by a factor of ~ 20 without impacting reionization science capabilities. This compression technique, which is based on delay/delay-rate filtering (**Parsons and Backer 2009**), is applied uniformly to all visibilities in the array, does not require (or produce) detailed calibration information, and is minimally restrictive for how data are analyzed and calibrated afterward. Data compression is run on the same GPU servers that implement the correlator X-Engines (§4.1.4). Since HERA only observes at night, these processors would otherwise be unused. UC Berkeley is responsible for porting the existing data compression pipeline to target these servers.

Data quality assurance (QA) is performed in real time on an additional modest computing cluster in the KAPB. UPenn leads the deployment and support of the hardware system that manages data transfer, applies routine calibration pipelines (see §4.3) and quality checks, and aggregates correlation-based metrics of array performance in real-time. The QA system furnishes this information into the separate monitor and control system (§4.1.6). A modest amount of data transfer is possible over the internet; PAPER’s data transfer rate from the Karoo to UPenn varies, but peaks around 40 Mbps. The QA system drives internet data transfer, but NAS devices and RAID storage, transferred by air-freight shipping, ensure full data transfer to UPenn.

4.1.6. Monitor and Control

The U. of Washington team leads the development of HERA’s Monitor and Control (M&C) system, which is a straightforward port of a similar system used on the MWA (**Tingay et al. 2013**). This system is responsible for tracking observing status, array startup and shutdown, and monitoring all active HERA systems. In the process, the M&C system builds a sizeable database of metadata that is crucial for verifying system functionality, identifying hardware failures, and feeding calibration and contextual information into data analysis pipelines.

4.2. Array Construction and Commissioning

The construction of HERA elements in the array consists of five primary steps: (1) site preparation and surveying, (2) pole installation by contracted labor with specialized utility pole equipment, (3) hub placement and height adjustment, (4) construction of full element using local labor, and

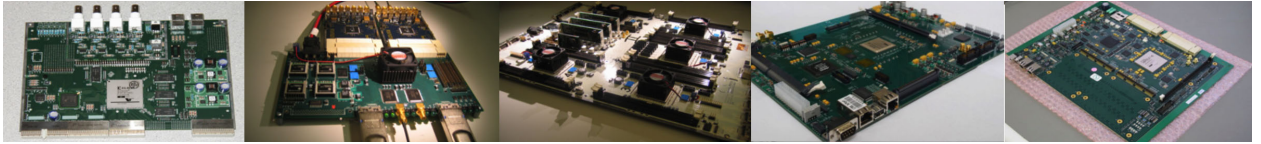


Fig. 14.— Five generations of CASPER technology (progressing left to right) have been used to rapidly develop, test, and deploy digital instrumentation for radio astronomy. This technology allows the PAPER correlator to be easily upgraded for HERA, incorporating new technology (Parsons et al. 2006, 2008).

(5) migration of PAPER dipoles to new ground screens by project staff. Contractors and immediate supervisors are based in South Africa. Supervision staff are part of the extensive support infrastructure in place on site associated with South African SKA activities. The PVC and wood sub-assemblies are constructed under contract off-site where material and labor are readily accessible. After shipment to site, the remaining construction involving sub-assemblies, pre-cut wood, PVC, and pre-cut wire cloth is done on-site under contract.

As construction proceeds incrementally, project staff begin migrating over existing PAPER feeds and cables and start commissioning the array. Commissioning activities are led first by subsystem owners, verifying that deployed subsystems continue to pass the test suites developed for the Critical Design Review. As the focus moves to system-level integration processes, downstream subsystems increasingly lead commissioning efforts until a subset of the HERA array has been fully integrated and tested. Once a baseline of functionality is established, more antennas and upgraded subsystems can be incorporated incrementally as they are available. These commissioning activities follow the successful build/commission model used by both PAPER and MWA, where observers tracked the incremental build-out process, performed observations in a “science-like mode,” and made adjustments as needed.

More advanced commissioning tasks involve all institutions, and focus on meeting top-level science requirements and resulting specifications. These tasks exercise the Monitor and Control subsystem (M&C; §4.1.6) and the Quality Assurance data processor (QA; §4.1.5), aggregating sources of information about array health from all subsystems and providing an accurate state of the system report visible and understandable to the entire project. Tests and pipelines developed during commissioning are folded into the routine analysis that reports to the M&C system. As systems stabilize, useful post-processing steps such as redundancy-based calibration and automated imaging are incorporated into the on-site QA server.

4.3. Software, Analysis, and Science

Beyond the construction and data-taking aspects of HERA, this proposal incorporates a full data analysis effort, culminating in the publication of a suite of science papers connecting observations to the physics of cosmic dawn. These efforts leverage existing software pipelines, with on-going development driven by students and postdocs targeting specific science goals. On the science side, HERA leverages the involvement of a team of theory collaborators, including Furlanetto, Lidz, Loeb, McQuinn, Mesinger, Oh, Pritchard, Santos, and Sutter.

Calibration and Snapshot Imaging. MIT leads the development of a real-time redundancy-based calibration pipeline based on related MITEoR and PAPER efforts. These instantaneous calibration solutions are provided to the Monitor and Control system to enable hardware misbehaviors to be quickly identified, and also support the real-time imaging pipeline. Absolute calibration is fixed with a combination of self-calibration techniques and absolutely calibrated baluns developed

at ASU and NRAO. Offline, detailed imaging efforts feed into developing empirical beam models that complement electromagnetic simulations. UPenn develops polarization beam models that determine whether polarization leakage can be formally retired as a risk and lay the foundation for imaging-based foreground suppression that corrects any remaining leakage effects.

Foreground Modeling. The U. Washington team leads the adaptation of a high dynamic-range imaging pipeline based on the Fast Holographic Deconvolution (FHD; **Sullivan et al. 2012**) for HERA. The full-Stokes sky maps resulting from this pipeline are used to directly subtract foregrounds and as data products themselves. UPenn leads the characterization of the polarized sky and the distribution of rotation measures. Data from HERA, PAPER, and the MWA are used to update source catalogs and a Global Sky Model (**de Oliveira-Costa et al. 2008**).

Power Spectra. UC Berkeley leads early power spectrum measurements using the conservative delay-spectrum approach used in PAPER. Development of the power-spectrum pipeline will focus on incorporating a fully covariant description of the foreground wedge (**Liu and Tegmark 2011; Dillon et al. 2013a**), as well as exploring Bayesian techniques for power spectrum estimation, building on the considerable progress already made on Gibbs-sampling imaging for interferometers (**Sutter et al. 2014**). In addition to the statistical foreground mitigation techniques provided by optimal quadratic power-spectrum estimation, U. Washington leads the application of foreground modeling for expanding the range of modes available for power spectrum analysis. Techniques developed should be equally applicable to measurements in both the reionization epoch and at higher redshifts. MIT leads the application of these tools for pre-reionization science.

Simulation. To provide verification of power spectrum constraints, ASU leads the development of an end-to-end simulator of the full HERA instrument, incorporating foregrounds and reionization models to output visibilities. UCLA also leads a parametrized reionization simulation effort that, coupled with the instrument simulator, is critical for connecting power-spectrum constraints to the estimation of the underlying astrophysical models.

HI Imaging. In addition to supplying models for suppressing foregrounds, deep imaging aims to map HI emission during reionization (see §2.1). Initially, conservative filtering of the foreground wedge is applied to data that are imaged. These results are compared with the residuals from imaging-based foreground suppression to explore the limitations of precision foreground imaging and removal. As imaging-based techniques mature, the resultant maps are released for cross-correlation with other probes of reionization.

5. Broader Impacts

At the core of HERA’s plan to broaden its impact is an international scientific collaboration and student exchange program with South Africa. We also continue the PAPER and MWA legacy of training new scientists and engineers at the undergraduate, graduate, and postdoctoral levels. We make major data products available publicly as a benefit to the community, and help to define the science context and techniques for the next generation of experiments — particularly the SKA.

5.1. South African Student Exchange

We propose a student exchange program between HERA and South African scientific collaborators, building on the existing collaboration between PAPER, CASPER, SKA-SA, and South African universities. We have identified several collaborators at SA institutions (see attached letters of support from Bernardi (SKA-SA); Chiang, Moodley, and Sievers (UKZN); Maartens and Santos

(UWC)). This exchange is mutually beneficial, preparing students on both sides as scientific and engineering leaders in next-generation 21 cm reionization experiments and the SKA. This exchange increases the size, diversity, and quality of US graduate programs by engaging and preparing South African students for admission to US institutions, and by exposing US students to the burgeoning radio astronomy facilities being developed in South Africa as part of the SKA.

Each year, 3–4 students from the USA and SA travel to a rotating host institution to work on a related set of research problems. Experience has shown that small groups facilitate peer mentoring and a sense of community, particularly when operating in a new cultural environment. A similar approach is taken for South African students in the National Astrophysics and Space Science Programme (NASSP) and also in US programs (e.g., the Posse Foundation). Over a three-month period, students interact with their host institution’s faculty, postdocs, and graduate students. Budget allowance includes travel, lodging, and meals. Master’s students are mentored for applying to Ph.D. programs and engineering positions. Doctoral candidates participate in multiple exchanges, establishing a scientific presence in their host country for building collaborations, applying for postdoctoral or permanent positions, and using the host country’s astronomy facilities.

This outreach program draws from an existing pool of talent, leveraging SKA-SA’s standing commitment to aiding previously disadvantaged South Africans, which prioritizes support to black and female South Africans at the undergraduate level, identifying non-traditional students, and guiding and supporting them into higher levels of research. Special attention is paid to bridging issues of scientific culture, allowing both groups to function at the highest possible level within their exchange community. We anticipate that this program will prepare students on both sides to be able to productively apply for graduate, postdoctoral, and faculty positions in the exchange country, and to effectively apply for observing time on the SKA and NRAO facilities.

5.2. Additional Broader Impacts and Previous Results

With each institution contributing subsystems to HERA, students and postdocs at all institutions take a leading role in development, testing, deployment, commissioning, and observing. This continues the HERA collaboration’s commitment to training a diverse set of students to become next-generation leaders in science. A prime example of this is CASPER, which began as the core of PAPER’s digital development effort, recruiting undergraduates, interns, grad students, and postdocs to work alongside seasoned RAL veteran engineers in a laboratory setting. CASPER now supports a global community of instrumentalists with a broad range of tools, including mailing lists, student visits, annual workshops, and an online repository of documentation and pedagogical materials. While grant support for CASPER at UC Berkeley has expired, this community continues to look to UC Berkeley’s leadership. Part of HERA’s broader impact continues this legacy, adapting technology developed for HERA for broader use in the CASPER community, hosting the workshops that help define this community, and continuing to recruit bright young students to develop novel approaches to scientific instrumentation.

HERA builds on a long history of student training, career development, and public outreach. PAPER and the MWA have included undergraduate, graduate, and postdoctoral researchers in all phases of design, construction, and analysis. The combined efforts of these groups have trained an impressive cadre of scientists skilled in instrumentation, data analysis, and theory, as well as engineers working at the forefront of digital technology. MITEoR has placed seven physics undergrads in competitive graduate schools. Over a dozen interns from South African universities have

received academic credit for participating in PAPER’s major engineering deployments. Furlanetto (UCLA) has led two summer REU projects and has presented his work to three astronomy clubs in the LA area. Aguirre’s (Penn) numerous undergraduate and high-school students working on PAPER include an Acorda Scientific Excellence Awardee. Parsons (UCB) routinely produces public (YouTube) pedagogical videos for undergraduate teaching, and has established an internship program for training budding instrumentalists. Morales (UW) was honored by Diversity Magazine as an emerging minority scholar, was featured in the Pacific Science Center’s “Scientists Like Me: Faces of Discovery”, and has implemented a successful community college transfer program. Bowman and Jacobs (ASU) are actively involved in community outreach at local urban schools and tribal centers. Hewitt (MIT) has a long history of advocating for women in science and has helped establish family leave policies for young faculty. Tegmark (MIT) has reached a wide lay audience through his popular book, “Our Mathematical Universe” (New York Times Bestseller’s List, Jan. 2014), which includes sections on radio instrumentation and 21 cm cosmology.

HERA collaborators have a strong record of sharing breakthrough innovations with the wider scientific and engineering communities, distributing open-source software (AIPY, DexM), hardware and firmware (CASPER), and instrument architectures (PAPER, LEDA, Omniscope), publishing innovative analysis approaches (FHD, MOFF, Omniscope), and serving in leadership roles for major international communities (SKA, ASKAP, ALMA, MeerKat, Chime). While HERA is an experiment rather than an observatory, its results are scientifically and technologically relevant for the SKA and for high-redshift observing with JWST and ALMA. As detailed in the Data Management Plan, HERA’s data products are made available to the wider community for a variety of studies, both those directly relevant to the cosmic dawn and other topics, such as transient studies.

6. Summary

This HERA proposal follows the vision for 21 cm observations laid out in NWNH, with the US EoR projects (PAPER, MWA, EDGES, MITEoR) pooling their expertise to develop a second-generation instrument. The resulting team comes with a deep well of scientific experience. This expertise has led to rapid progress in the last few years, with current instruments having fulfilled their primary goal envisioned in NWNH: characterizing and suppressing astrophysical foregrounds through hardware and analysis development to the point where thermal noise limits have been reached. MWA, PAPER, and LOFAR are now pushing hard to detect the EoR power spectrum, but at best, the detection will be marginal. Through judicious leveraging of the EoR window and related foreground mitigation techniques, HERA not only ensures a high significance detection of the HI 21 cm signal, but also provides strong constraints on the reionization history, early structure formation, and heating processes at the end of the cosmic dark ages. This proposal comes at an opportune time in the field, picking up where PAPER, the MWA, and LOFAR leave off, and delivering results on a timescale that ensures continued US leadership in the field.

Studying the formation of the first luminous structures and how they reionize the Universe is a primary driver for nearly all major astronomical facilities over the next decade. Such studies include direct observations of stars, gas, dust, and AGN in the first galaxies using the JWST, TMT, and ALMA. HERA is a necessary element in this panchromatic arsenal, providing a unique window into the impact of these sources on their large-scale environments.

References

- Bolton, J. S., M. G. Haehnelt, S. J. Warren, P. C. Hewett, D. J. Mortlock, B. P. Venemans, R. G. McMahon, and C. Simpson, 2011: How neutral is the intergalactic medium surrounding the redshift $z = 7.085$ quasar ULAS J1120+0641? *MNRAS*, **416**, L70–L74, 1106.6089.
- Bouwens, R. J., G. D. Illingworth, P. A. Oesch, M. Stiavelli, P. van Dokkum, M. Trenti, D. Magee, I. Labb  , M. Franx, C. M. Carollo, and V. Gonzalez, 2010: Discovery of $z \sim 8$ Galaxies in the Hubble Ultra Deep Field from Ultra-Deep WFC3/IR Observations. *ApJ*, **709**, L133–L137, 0909.1803.
- Bowman, J. D., M. F. Morales, and J. N. Hewitt, 2009: Foreground Contamination in Interferometric Measurements of the Redshifted 21 cm Power Spectrum. *ApJ*, **695**, 183–199, 0807.3956.
- Clark, M. A., P. C. La Plante, and L. J. Greenhill, 2011: Accelerating Radio Astronomy Cross-Correlation with Graphics Processing Units. *ArXiv e-prints*, 1107.4264.
- Committee for a Decadal Survey of A&A; NRC, 2010: *New Worlds, New Horizons in Astronomy and Astrophysics*. Natl. Academies Press.
- Datta, A., J. D. Bowman, and C. L. Carilli, 2010: Bright Source Subtraction Requirements for Redshifted 21 cm Measurements. *ApJ*, **724**, 526–538, 1005.4071.
- de Oliveira-Costa, A., M. Tegmark, B. M. Gaensler, J. Jonas, T. L. Landecker, and P. Reich, 2008: A model of diffuse Galactic radio emission from 10 MHz to 100 GHz. *MNRAS*, **388**, 247–260, arXiv:0802.1525.
- Dillon, J. S., A. Liu, and M. Tegmark, 2013a: A fast method for power spectrum and foreground analysis for 21 cm cosmology. *Phys. Rev. D*, **87**(4), 043005, 1211.2232.
- Dillon, J. S., A. Liu, C. L. Williams, J. N. Hewitt, M. Tegmark, E. H. Morgan, A. M. Levine, M. F. Morales, S. J. Tingay, G. Bernardi, J. D. Bowman, F. H. Briggs, D. Emrich, D. A. Mitchell, D. Oberoi, T. Prabu, R. Wayth, and R. L. Webster, 2013b: Overcoming real-world obstacles in 21 cm power spectrum estimation: A method demonstration and results from early Murchison Widefield Array data. *ArXiv*, 1304.4229.
- Ellis, R. S., R. J. McLure, J. S. Dunlop, B. E. Robertson, Y. Ono, M. A. Schenker, A. Koekemoer, R. A. A. Bowler, M. Ouchi, A. B. Rogers, E. Curtis-Lake, E. Schneider, S. Charlot, D. P. Stark, S. R. Furlanetto, and M. Cirasuolo, 2013: The Abundance of Star-forming Galaxies in the Redshift Range 8.5–12: New Results from the 2012 Hubble Ultra Deep Field Campaign. *ApJ*, **763**, L7, 1211.6804.
- Faisst, A. L., P. Capak, C. M. Carollo, C. Scarlata, and N. Scoville, 2014: Spectroscopic observation of Ly α emitters at $z \sim 7.7$ and implications on re-ionization. *ArXiv e-prints*, 1402.3604.
- Fan, X., C. L. Carilli, and B. Keating, 2006: Observational Constraints on Cosmic Reionization. *ARA&A*, **44**, 415–462, arXiv:astro-ph/0602375.
- Furlanetto, S. R., S. P. Oh, and F. H. Briggs, 2006: Cosmology at low frequencies: The 21 cm transition and the high-redshift Universe. *Phys. Rep.*, **433**, 181–301, arXiv:astro-ph/0608032.
- Furlanetto, S. R., M. Zaldarriaga, and L. Hernquist, 2004: The Growth of H II Regions During Reionization. *ApJ*, **613**, 1–15, arXiv:astro-ph/0403697.
- Gong, Y., A. Cooray, M. B. Silva, M. G. Santos, and P. Lubin, 2011: Probing Reionization with Intensity Mapping of Molecular and Fine-structure Lines. *ApJ*, **728**, L46, 1101.2892.
- Haiman, Z. and A. Loeb, 1997: Signatures of Stellar Reionization of the Universe. *ApJ*, **483**, 21, arXiv:astro-ph/9611028.

- Harker, G., S. Zaroubi, G. Bernardi, M. A. Brentjens, A. G. de Bruyn, B. Ciardi, V. Jelić, L. V. E. Koopmans, P. Labropoulos, G. Mellema, A. Offringa, V. N. Pandey, J. Schaye, R. M. Thomas, and S. Yatawatta, 2009: Non-parametric foreground subtraction for 21-cm epoch of reionization experiments. *MNRAS*, **397**, 1138–1152, 0903.2760.
- Hazelton, B. J., M. F. Morales, and I. S. Sullivan, 2013: The Fundamental Multi-Baseline Mode-Mixing Foreground in 21 cm EoR Observations. *ArXiv*, 1301.3126.
- Jelić, V., S. Zaroubi, P. Labropoulos, G. Bernardi, A. G. de Bruyn, and L. V. E. Koopmans, 2010: Realistic simulations of the Galactic polarized foreground: consequences for 21-cm reionization detection experiments. *MNRAS*, **409**, 1647–1659, 1007.4135.
- Jelić, V., S. Zaroubi, P. Labropoulos, R. M. Thomas, G. Bernardi, M. A. Brentjens, A. G. de Bruyn, B. Ciardi, G. Harker, L. V. E. Koopmans, V. N. Pandey, J. Schaye, and S. Yatawatta, 2008: Foreground simulations for the LOFAR-epoch of reionization experiment. *MNRAS*, **389**, 1319–1335, 0804.1130.
- Labropoulos, P., L. V. E. Koopmans, V. Jelic, S. Yatawatta, R. M. Thomas, G. Bernardi, M. Brentjens, G. de Bruyn, B. Ciardi, G. Harker, A. Offringa, V. N. Pandey, J. Schaye, and S. Zaroubi, 2009: The LOFAR EoR Data Model: (I) Effects of Noise and Instrumental Corruptions on the 21-cm Reionization Signal-Extraction Strategy. *ArXiv e-prints*, 0901.3359.
- Lidz, A., S. R. Furlanetto, S. P. Oh, J. Aguirre, T.-C. Chang, O. Doré, and J. R. Pritchard, 2011: Intensity Mapping with Carbon Monoxide Emission Lines and the Redshifted 21 cm Line. *ApJ*, **741**, 70, 1104.4800.
- Lidz, A., O. Zahn, S. R. Furlanetto, M. McQuinn, L. Hernquist, and M. Zaldarriaga, 2009: Probing Reionization with the 21 cm Galaxy Cross-Power Spectrum. *ApJ*, **690**, 252–266, 0806.1055.
- Liu, A. and M. Tegmark, 2011: A method for 21 cm power spectrum estimation in the presence of foregrounds. *Phys. Rev. D*, **83(10)**, 103006, 1103.0281.
- Liu, A., M. Tegmark, S. Morrison, A. Lutomirski, and M. Zaldarriaga, 2010: Precision calibration of radio interferometers using redundant baselines. *MNRAS*, **408**, 1029–1050, 1001.5268.
- Liu, A., M. Tegmark, and M. Zaldarriaga, 2008: Will point sources spoil 21 cm tomography? *ArXiv*, 0807.3952.
- McQuinn, M., A. Lidz, O. Zahn, S. Dutta, L. Hernquist, and M. Zaldarriaga, 2007: The morphology of HII regions during reionization. *MNRAS*, **377**, 1043–1063, arXiv:astro-ph/0610094.
- Mesinger, A., A. Ferrara, and D. S. Spiegel, 2013: Signatures of X-rays in the early Universe. *MNRAS*, **431**, 621–637, 1210.7319.
- Mesinger, A. and S. Furlanetto, 2007: Efficient Simulations of Early Structure Formation and Reionization. *ApJ*, **669**, 663–675, 0704.0946.
- Mesinger, A., S. Furlanetto, and R. Cen, 2011: 21CMFAST: a fast, seminumerical simulation of the high-redshift 21-cm signal. *MNRAS*, **411**, 955–972, 1003.3878.
- Mesinger, A., M. McQuinn, and D. N. Spergel, 2012: The kinetic Sunyaev-Zel'dovich signal from inhomogeneous reionization: a parameter space study. *MNRAS*, **422**, 1403–1417, 1112.1820.
- Moore, D. F., J. E. Aguirre, A. R. Parsons, D. C. Jacobs, and J. C. Pober, 2013: The Effects of Polarized Foregrounds on 21 cm Epoch of Reionization Power Spectrum Measurements. *ApJ*, **769**, 154, 1302.0876.
- Morales, M. F., J. D. Bowman, and J. N. Hewitt, 2006: Improving Foreground Subtraction in Statistical Observations of 21 cm Emission from the Epoch of Reionization. *ApJ*, **648**, 767–773,

arXiv:astro-ph/0510027.

- Morales, M. F., B. Hazelton, I. Sullivan, and A. Beardsley, 2012: Four Fundamental Foreground Power Spectrum Shapes for 21 cm Cosmology Observations. *ApJ*, **752**, 137, 1202.3830.
- Morales, M. F. and J. S. B. Wyithe, 2010: Reionization and Cosmology with 21-cm Fluctuations. *ARA&A*, **48**, 127–171, 0910.3010.
- Oesch, P. A., R. J. Bouwens, G. D. Illingworth, I. Labb , M. Franx, P. G. van Dokkum, M. Trenti, M. Stiavelli, V. Gonzalez, and D. Magee, 2013: Probing the Dawn of Galaxies at $z \sim 9\text{--}12$: New Constraints from HUDF12/XDF and CANDELS data. *ApJ*, **773**, 75, 1301.6162.
- Page, L., G. Hinshaw, E. Komatsu, M. R. Nolta, D. N. Spergel, C. L. Bennett, C. Barnes, R. Bean, O. Dor , J. Dunkley, M. Halpern, R. S. Hill, N. Jarosik, A. Kogut, M. Limon, S. S. Meyer, N. Odegard, H. V. Peiris, G. S. Tucker, L. Verde, J. L. Weiland, E. Wollack, and E. L. Wright, 2007: Three-Year Wilkinson Microwave Anisotropy Probe (WMAP) Observations: Polarization Analysis. *ApJS*, **170**, 335–376, arXiv:astro-ph/0603450.
- Parsons, A., D. Backer, C. Chang, D. Chapman, H. Chen, P. Crescini, C. de Jesus, C. Dick, P. Droz, D. MacMahon, K. Meder, J. Mock, V. Nagpal, B. Nikolic, A. Parsa, B. Richards, A. Siemion, J. Wawrynek, D. Werthimer, and M. Wright, 2006: PetaOp/Second FPGA Signal Processing for SETI and Radio Astronomy. In *Asilomar Conference on Signals and Systems, Pacific Grove, CA*, pp. 2031–2035.
- Parsons, A., D. Backer, A. Siemion, H. Chen, D. Werthimer, P. Droz, T. Filiba, J. Manley, P. MacMahon, A. Parsa, D. MacMahon, and M. Wright, 2008: A Scalable Correlator Architecture Based on Modular FPGA Hardware, Reuseable Gateware, and Data Packetization. *PASP*, **120**, 1207–1221, 0809.2266.
- Parsons, A., J. Pober, M. McQuinn, D. Jacobs, and J. Aguirre, 2012a: A Sensitivity and Array-configuration Study for Measuring the Power Spectrum of 21 cm Emission from Reionization. *ApJ*, **753**, 81, 1103.2135.
- Parsons, A. R. and D. C. Backer, 2009: Calibration of Low-Frequency, Wide-Field Radio Interferometers Using Delay/Delay-Rate Filtering. *AJ*, **138**, 219–226, 0901.2575.
- Parsons, A. R., D. C. Backer, G. S. Foster, M. C. H. Wright, R. F. Bradley, N. E. Gugliucci, C. R. Parashare, E. E. Benoit, J. E. Aguirre, D. C. Jacobs, C. L. Carilli, D. Herne, M. J. Lynch, J. R. Manley, and D. J. Werthimer, 2010: The Precision Array for Probing the Epoch of Re-ionization: Eight Station Results. *AJ*, **139**, 1468–1480, 0904.2334.
- Parsons, A. R., A. Liu, J. E. Aguirre, Z. S. Ali, R. F. Bradley, C. L. Carilli, D. R. DeBoer, M. R. Dexter, N. E. Gugliucci, D. C. Jacobs, P. Klima, D. H. E. MacMahon, J. R. Manley, D. F. Moore, J. C. Pober, I. I. Stefan, and W. P. Walbrugh, 2013: New Limits on 21cm EoR From PAPER-32 Consistent with an X-Ray Heated IGM at $z=7.7$. *ArXiv*, 1304.4991.
- Parsons, A. R., J. C. Pober, J. E. Aguirre, C. L. Carilli, D. C. Jacobs, and D. F. Moore, 2012b: A Per-baseline, Delay-spectrum Technique for Accessing the 21 cm Cosmic Reionization Signature. *ApJ*, **756**, 165, 1204.4749.
- Planck Collaboration, P. A. R. Ade, N. Aghanim, C. Armitage-Caplan, M. Arnaud, M. Ashdown, F. Atrio-Barandela, J. Aumont, C. Baccigalupi, A. J. Banday, and et al., 2013: Planck 2013 results. XVI. Cosmological parameters. *ArXiv*, 1303.5076.
- Pober, J. C., A. Liu, J. S. Dillon, J. E. Aguirre, J. D. Bowman, R. F. Bradley, C. L. Carilli, D. R. DeBoer, J. N. Hewitt, D. C. Jacobs, M. McQuinn, M. F. Morales, A. R. Parsons, M. Tegmark,

- and D. J. Werthimer, 2014: What Next-generation 21 cm Power Spectrum Measurements can Teach us About the Epoch of Reionization. *ApJ*, **782**, 66, 1310.7031.
- Pober, J. C., A. R. Parsons, J. E. Aguirre, Z. Ali, R. F. Bradley, C. L. Carilli, D. DeBoer, M. Dexter, N. E. Gugliucci, D. C. Jacobs, P. J. Klima, D. MacMahon, J. Manley, D. F. Moore, I. I. Stefan, and W. P. Walbrugh, 2013: Opening the 21 cm Epoch of Reionization Window: Measurements of Foreground Isolation with PAPER. *ApJ*, **768**, L36, 1301.7099.
- Pritchard, J. R. and A. Loeb, 2010: Constraining the unexplored period between the dark ages and reionization with observations of the global 21 cm signal. *Phys. Rev. D*, **82**(2), 023006, 1005.4057.
- Robertson, B. E., S. R. Furlanetto, E. Schneider, S. Charlot, R. S. Ellis, D. P. Stark, R. J. McLure, J. S. Dunlop, A. Koekemoer, M. A. Schenker, M. Ouchi, Y. Ono, E. Curtis-Lake, A. B. Rogers, R. A. A. Bowler, and M. Cirasuolo, 2013: New Constraints on Cosmic Reionization from the 2012 Hubble Ultra Deep Field Campaign. *ApJ*, **768**, 71, 1301.1228.
- Santos, M. G., L. Ferramacho, M. B. Silva, A. Amblard, and A. Cooray, 2010: Fast large volume simulations of the 21-cm signal from the reionization and pre-reionization epochs. *MNRAS*, **406**, 2421–2432, 0911.2219.
- Schenker, M. A., B. E. Robertson, R. S. Ellis, Y. Ono, R. J. McLure, J. S. Dunlop, A. Koekemoer, R. A. A. Bowler, M. Ouchi, E. Curtis-Lake, A. B. Rogers, E. Schneider, S. Charlot, D. P. Stark, S. R. Furlanetto, and M. Cirasuolo, 2013: The UV Luminosity Function of Star-forming Galaxies via Dropout Selection at Redshifts $z \sim 7$ and 8 from the 2012 Ultra Deep Field Campaign. *ApJ*, **768**, 196, 1212.4819.
- Shapiro, P. R. and M. L. Giroux, 1987: Cosmological H II regions and the photoionization of the intergalactic medium. *ApJ*, **321**, L107–L112.
- Silva, M. B., M. G. Santos, Y. Gong, A. Cooray, and J. Bock, 2013: Intensity Mapping of Ly α Emission during the Epoch of Reionization. *ApJ*, **763**, 132, 1205.1493.
- Sullivan, I. S., M. F. Morales, B. J. Hazelton, W. Arcus, D. Barnes, G. Bernardi, F. H. Briggs, J. D. Bowman, J. D. Bunton, R. J. Cappallo, B. E. Corey, A. Deshpande, L. deSouza, D. Emrich, B. M. Gaensler, R. Goeke, L. J. Greenhill, D. Herne, J. N. Hewitt, M. Johnston-Hollitt, D. L. Kaplan, J. C. Kasper, B. B. Kincaid, R. Koenig, E. Kratzenberg, C. J. Lonsdale, M. J. Lynch, S. R. McWhirter, D. A. Mitchell, E. Morgan, D. Oberoi, S. M. Ord, J. Pathikulangara, T. Prabu, R. A. Remillard, A. E. E. Rogers, A. Roshi, J. E. Salah, R. J. Sault, N. Udaya Shankar, K. S. Srivani, J. Stevens, R. Subrahmanyan, S. J. Tingay, R. B. Wayth, M. Waterson, R. L. Webster, A. R. Whitney, A. Williams, C. L. Williams, and J. S. B. Wyithe, 2012: Fast Holographic Deconvolution: A New Technique for Precision Radio Interferometry. *ApJ*, **759**, 17, 1209.1653.
- Sutter, P. M., B. D. Wandelt, J. D. McEwen, E. F. Bunn, A. Karakci, A. Korotkov, P. Timbie, G. S. Tucker, and L. Zhang, 2014: Probabilistic image reconstruction for radio interferometers. *MNRAS*, **438**, 768–778, 1309.1469.
- Tingay, S. J., R. Goeke, J. D. Bowman, D. Emrich, S. M. Ord, D. A. Mitchell, M. F. Morales, T. Booler, B. Crosse, R. B. Wayth, C. J. Lonsdale, S. Tremblay, D. Pallot, T. Colegate, A. Wicenec, N. Kudryavtseva, W. Arcus, D. Barnes, G. Bernardi, F. Briggs, S. Burns, J. D. Bunton, R. J. Cappallo, B. E. Corey, A. Deshpande, L. Desouza, B. M. Gaensler, L. J. Greenhill, P. J. Hall, B. J. Hazelton, D. Herne, J. N. Hewitt, M. Johnston-Hollitt, D. L. Kaplan, J. C. Kasper, B. B. Kincaid, R. Koenig, E. Kratzenberg, M. J. Lynch, B. McKinley, S. R. McWhirter,

- E. Morgan, D. Oberoi, J. Pathikulangara, T. Prabu, R. A. Remillard, A. E. E. Rogers, A. Roshi, J. E. Salah, R. J. Sault, N. Udaya-Shankar, F. Schlagenhauf, K. S. Srivani, J. Stevens, R. Subrahmanyan, M. Waterson, R. L. Webster, A. R. Whitney, A. Williams, C. L. Williams, and J. S. B. Wyithe, 2013: The Murchison Widefield Array: The Square Kilometre Array Precursor at Low Radio Frequencies. *PASA*, **30**, 7, 1206.6945.
- Treu, T., K. B. Schmidt, M. Trenti, L. D. Bradley, and M. Stiavelli, 2013: The changing Ly α optical depth in the range $6 < z < 9$ from MOSFIRE spectroscopy of Y-dropouts. *ArXiv*, 1308.5985.
- Vedantham, H., N. Udaya Shankar, and R. Subrahmanyan, 2012: Imaging the Epoch of Reionization: Limitations from Foreground Confusion and Imaging Algorithms. *ApJ*, **745**, 176, 1106.1297.
- Visbal, E., R. Barkana, A. Fialkov, D. Tseliakhovich, and C. M. Hirata, 2012: The signature of the first stars in atomic hydrogen at redshift 20. *Nature*, **487**, 70–73, 1201.1005.
- Wiersma, R. P. C., B. Ciardi, R. M. Thomas, G. J. A. Harker, S. Zaroubi, G. Bernardi, M. Brentjens, A. G. de Bruyn, S. Daiboo, V. Jelic, S. Kazemi, L. V. E. Koopmans, P. Labropoulos, O. Martinez, G. Mellema, A. Offringa, V. N. Pandey, J. Schaye, V. Veligatla, H. Vedantham, and S. Yatawatta, 2013: LOFAR insights into the epoch of reionization from the cross-power spectrum of 21 cm emission and galaxies. *MNRAS*, **432**, 2615–2624, 1209.5727.
- Zahn, O., C. L. Reichardt, L. Shaw, A. Lidz, K. A. Aird, B. A. Benson, L. E. Bleem, J. E. Carlstrom, C. L. Chang, H. M. Cho, T. M. Crawford, A. T. Crites, T. de Haan, M. A. Dobbs, O. Doré, J. Dudley, E. M. George, N. W. Halverson, G. P. Holder, W. L. Holzapfel, S. Hoover, Z. Hou, J. D. Hrubes, M. Joy, R. Keisler, L. Knox, A. T. Lee, E. M. Leitch, M. Lueker, D. Luong-Van, J. J. McMahon, J. Mehl, S. S. Meyer, M. Millea, J. J. Mohr, T. E. Montroy, T. Natoli, S. Padin, T. Plagge, C. Pryke, J. E. Ruhl, K. K. Schaffer, E. Shirokoff, H. G. Spieler, Z. Staniszewski, A. A. Stark, K. Story, A. van Engelen, K. Vanderlinde, J. D. Vieira, and R. Williamson, 2012: Cosmic Microwave Background Constraints on the Duration and Timing of Reionization from the South Pole Telescope. *ApJ*, **756**, 65, 1111.6386.